A hierarchy of Eulerian models for trajectory crossing in particle-laden turbulent flows over a wide range of Stokes numbers

By F. Laurent, A. Vié, C. Chalons, R. O. Fox AND M. Massot

1. Motivation and objective

With the large increase in available computational resources, large-eddy simulation (LES) of industrial configurations has become an efficient and tractable alternative to traditional multiphase turbulence models. Many applications involve a liquid or solid disperse phase carried by a gas phase (e.g., fuel injection in automotive or aeronautical engines, fluidized beds, and alumina particles in rocket boosters). To simulate such flows, one may resort to a number density function (NDF) for the disperse phase that satisfies a kinetic equation. Solving for the NDF can make use of Lagrangian Monte-Carlo methods, but such approaches are expensive, especially for unsteady flows, as the amount of numerical particles needed to control statistical errors is large. Moreover, such methods are not well adapted to high-performance computing because of the intrinsic spatial inhomogeneity of the NDF in most of the applications of interest. To overcome these issues, one can resort to Eulerian methods that solve for the moments of the NDF using an Eulerian system of conservation laws.

In the context of direct-numerical simulation (DNS), Février *et al.* (2005) introduced the mesoscopic Eulerian formalism (MEF). It yields a statistical decomposition of the motion of particles into correlated and uncorrelated parts, the former being common to all particles at a specific location, and the latter being induced by the history of each particle as it crosses different vortices before reaching a specific location. This decomposition induces unclosed stresses in the moment conservation equations. In Kaufmann *et al.* (2008) and more recently in Masi *et al.* (2011), algebraic-closure-based moment methods (ACBMM) are used to close these stresses: while solving for the random uncorrelated energy (i.e., granular energy), they provide constitutive closures to model the second-order moments. These closures are efficient at moderate Stokes numbers (Dombard 2011; Sierra 2012), for which particle trajectory crossings (PTC) occur at small scales, which are efficiently reproduced by second-order moments. However, at high Stokes numbers, this description of PTC is not satisfactory, as the correlated part of the motion will encounter large-scale PTC, the accurate representation of which requires high-order moments methods.

To solve for high-order moments, kinetics-based moment methods (KBMM) can be employed (Desjardins *et al.* 2008; Kah *et al.* 2010; Chalons *et al.* 2010; Yuan & Fox 2011; Chalons *et al.* 2012; Vié *et al.* 2011, 2012*b*,*a*). The main idea behind KBMM is to provide a presumed velocity distribution at the kinetic level potentially conditioned on size, which has as many parameters as the required number of moments. The presumed profile must be chosen carefully and should lead to simple algorithms in order to reconstruct the NDF from the moments, but also has to be based on physical arguments. In the context of small-scale PTC, the anisotropic Gaussian (AG) closure designed by Vié *et al.* (2012*a*)

can be used, which controls all second-order moments. A comparison between ACBMM and AG is provided in Vié *et al.* (2012*b*). For large-scale PTC, a sum of Dirac δ-functions can be used to account for the multi-modal velocity distribution at the crossing location. In 3-D, the conditional quadrature method of moments (CQMOM) of Yuan & Fox (2011) provides a fast inversion algorithm, and has demonstrated its ability in Taylor-Green flows. However, CQMOM has an important drawback: the related system of equations is weakly hyperbolic, meaning that it can generate unphysical δ-shocks. They refer to rapid accumulation of particles, when more than two trajectories cross, as mathematically analyzed by Chalons *et al.* (2012).

To overcome this issue, Chalons *et al.* (2010) have proposed the multi-Gaussian (MG) quadrature. Instead of using Dirac δ-functions as a kernel, Gaussian functions are used. In 1-D, by assuming equal variances for each Gaussian node, these authors provide a direct algorithm for the inversion. The resulting system of equations has three main properties: (1) it is hyperbolic, (2) in the limit of one node it degenerates towards the Gaussian distribution, ensuring the description of small-scale and large-scale PTC, and (3) in the context of LES, it can account for the velocity dispersion induced by subgrid scales of the turbulence thanks to the Gaussian kernel. In 2-D and 3-D, the MG algorithm has been extended using the idea behind CQMOM (Vié *et al.* 2011). The final method has been evaluated in Taylor-Green flow, where it has shown its potential.

The aim of this work is to apply the MG quadrature to more complex 2-D cases, to demonstrate its ability to avoid δ-shocks, and to capture additional dynamics as compared to standard KBMM using AG or CQMOM. We begin by introducing the kinetic equation and its related moment problem. Then we describe briefly the 2-D MG quadrature that is used to close the moment problem and the related algorithms used for moment evolution. Finally, the full method is applied on 2-D frozen homogeneous isotropic turbulence (HIT), and compared to AG, CQMOM and Lagrangian results.

2. The moment problem

In this work, we solve for the NDF $f(t, \mathrm{x}, \mathrm{v})$, at time t as a function of droplet position $\mathrm{x} = (x, y)^t$ and velocity $\mathrm{v} = (u, v)^t$, using a 2-D kinetic equation:

$$\partial_t f + \mathrm{v} \cdot \partial_{\mathrm{x}} f + \partial_{\mathrm{v}} \cdot (\mathrm{F} f) = 0, \quad t > 0,\ \mathrm{x} \in \mathbb{R}^2,\ \mathrm{v} \in \mathbb{R}^2, \tag{2.1}$$

where $\partial_{\mathrm{x}} = (\partial_x, \partial_y)^t$, $\partial_{\mathrm{v}} = (\partial_u, \partial_v)^t$ and $\mathrm{F} = (F_u, F_v)^t$ is the acceleration due to the drag force. As we consider Stokes drag, the acceleration due to drag is $\mathrm{F} = (\mathrm{v}_g - \mathrm{v})/\tau_p$, where $\mathrm{v}_g = (u_g, v_g)^t$ is the gas velocity and τ_p, the relaxation time. We define the bivariate moments of order (i, j) as $M_{i,j}(t, \mathrm{x}) = \int_{\mathbb{R}^2} u^i v^j f(t, \mathrm{x}, \mathrm{v})\, \mathrm{dv}$. The associated governing equations are easily obtained from Eq. (2.1):

$$\partial_t M_{i,j} + \partial_x M_{i+1,j} + \partial_y M_{i,j+1} = \frac{1}{\tau_p} \left[i M_{i-1,j} u_g + j M_{i,j-1} v_g - (i + j) M_{i,j} \right]. \tag{2.2}$$

There are two main issues with this type of model: the closure of the moment hierarchy and the numerical scheme. Indeed, for any given set of moments, there are always some fluxes that are not in closed form. To close the system, we use a reconstruction of the NDF at the kinetic level starting from a finite moment set. The choice of the reconstruction imposes the number of moments needed and induces the hyperbolicity or weak hyperbolicity property of the system. Moreover a kinetic finite volume scheme is used for convection, which makes use of the reconstruction to compute the unknown fluxes. For

the drag force terms, all moments are closed. However, the reconstruction is still useful to derive a quadrature approximation of these terms in case of arbitrary drag laws.

3. 2-D extended quadrature-based reconstruction

Treatment of particle-laden flows with LES over a wide range of Stokes numbers requires a quadrature reconstruction that can treat both large-scale and small-scale PTC. In this work we employ a 2-D extended version of the MG quadrature developed by Chalons *et al.* (2010), which can degenerate into two simpler quadratures, namely CQMOM (Yuan & Fox 2011) and anisotropic Gaussian (AG) (Vié *et al.* 2012*a*).

3.1. *MG quadrature*

The 2-D MG extended quadrature is constructed using the conditional moment algorithm described by Yuan & Fox (2011) and is found by conditioning, for example, the v velocity on the u velocity, or more precisely, conditioning a linear combination $v - a_0 - a_1 u$ on u†:

$$f_{12}(\mathrm{v}) = \sum_{\alpha=1}^{2}\sum_{\beta=1}^{2} \rho_\alpha \rho_{\alpha\beta} g(u; u_\alpha, \sigma_1) g(v; a_0 + a_1 u + v_{\alpha\beta}, \sigma_{2\alpha}), \tag{3.1}$$

where ρ_α, u_α and σ_1 are found using 1-D bi-Gaussian quadrature (Chalons *et al.* 2010) with the univariate moments $M_{i,0}$ for $i \in (0, 1, 2, 3, 4)$. (The definition of $f_{21}(\mathrm{v})$ is found by permuting u and v.) The Gaussian KDF is defined by

$$g(u; \mu, \sigma) = \frac{1}{\sigma\sqrt{2\pi}} \exp\left[-\frac{(u-\mu)^2}{2\sigma^2}\right],$$

and a_0 and a_1 are defined so that the moments of order $(0, 1)$ and $(1, 1)$ of f_{12} are $M_{0,1}$ and $M_{1,1}$. They are then found from the linear system

$$\begin{bmatrix} M_{0,0} & M_{1,0} \\ M_{1,0} & M_{2,0} \end{bmatrix} \begin{bmatrix} a_0 \\ a_1 \end{bmatrix} = \begin{bmatrix} M_{0,1} \\ M_{1,1} \end{bmatrix}.$$

The function f_{12} of Eq. (3.1) is then a sum of multi-variate Gaussian distributions centered at $(u_\alpha, v_{\alpha\beta} + a_0 + a_1 u_\alpha)$ with covariance matrices defined such that the diagonal terms are σ_1^2 and $\sigma_{2\alpha}^2 + a_1^2 \sigma_1^2$ and the off-diagonal term is $a_1 \sigma_1^2$. The dispersion of each Gaussian represents small-scale PTC whereas the dispersion of their centers represents large-scale PTC. The integer moments of f_{12} are

$$M_{i,j} = \sum_{\alpha=1}^{2} \rho_\alpha \sum_{k=0}^{j} \binom{j}{k} a_1^{j-k} \langle u^{i+j-k} \rangle_\alpha \mu_\alpha^k, \tag{3.2}$$

where the so-called conditional moments μ_α^k and $\langle u^i \rangle_\alpha$ are defined by

$$\mu_\alpha^k = \sum_{\beta=1}^{2} \rho_{\alpha\beta} \int_{\mathbb{R}} y^k g(y; v_{\alpha\beta} + a_0, \sigma_{2\alpha})\, \mathrm{d}y, \qquad \langle u^i \rangle_\alpha = \int_{\mathbb{R}} u^i g(u; u_\alpha, \sigma_1)\, \mathrm{d}u.$$

By definition, $\mu_\alpha^0 = 1$ and $\mu_\alpha^1 = a_0$. Thus, the linear system in Eq. (3.2) with $i = 0, 1$:

$$\begin{bmatrix} \rho_1 & \rho_2 \\ \rho_1 u_1 & \rho_2 u_2 \end{bmatrix} \begin{bmatrix} \mu_1^j \\ \mu_2^j \end{bmatrix} = \begin{bmatrix} M_{0,j} - \sum_{\alpha=1}^{2} \rho_\alpha \sum_{k=0}^{j-1} \binom{j}{k} \langle u^{i-k} \rangle_\alpha \mu_\alpha^k \\ M_{1,j} - \sum_{\alpha=1}^{2} \rho_\alpha \sum_{k=0}^{j-1} \binom{j}{k} \langle u^{i+1-k} \rangle_\alpha \mu_\alpha^k \end{bmatrix}$$

† It is a way to introduce some correlation between the u velocity and the v velocity inside each term of the sum, still using the conditional moment algorithm.

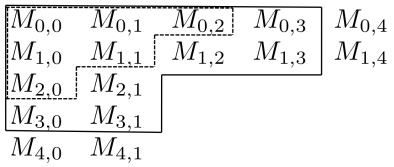

FIGURE 1. Moments needed for MG (all), CQMOM (solid line), AG (dashed line).

can be solved sequentially for $j = 2, 3, 4$ to find the unknown conditional moments. Finally, for $\alpha = 1, 2$ the conditional moment set $(\mu_\alpha^0, \mu_\alpha^1, \mu_\alpha^2, \mu_\alpha^3, \mu_\alpha^4)$ is used with 1-D bi-Gaussian quadrature (Chalons *et al.* 2010) to find $\rho_{\alpha\beta}$, $v_{\alpha\beta}$ and $\sigma_{2\alpha}$. In total, the sixteen bivariate moments needed to construct f_{12} and f_{21} (shown in Figure 1) are found by solving Eq. (2.2). We denote by $\mathcal{I}_{MG}$ the set of indices for these moments.

3.2. *Limiting cases*

The 2-D MG extended quadrature in Eq. (3.1) contains two important limiting cases corresponding to high and low Stokes numbers, respectively. For high Stokes numbers, the PTC is fully resolved and the modeled small-scale PTC is negligible. This corresponds to setting $\sigma_1 = \sigma_{2\alpha} = 0$, leading to

$$f_{12}(\mathrm{v}) = \sum_{\alpha=1}^{2} \rho_\alpha \delta(u - u_\alpha) \sum_{\beta=1}^{2} \rho_{\alpha\beta} \delta(v - a_0 - a_1 u - v_{\alpha\beta}), \tag{3.3}$$

which is a variation of CQMOM (Yuan & Fox 2011). In this limit, the ten solved moments are contained inside the solid line in Figure 1 and their indices live in $\mathcal{I}_{CQMOM} = \mathcal{I}_{MG} \backslash \{(4,0), (0,4), (4,1), (1,4)\}$. The remaining parameters in Eq. (3.3) are determined from the ten integer moments as described above.

For low Stokes numbers, large-scale PTC is negligible, which corresponds to setting $\rho_2 = \rho_{12} = 0$ in the 2-D MG quadrature. This leads to the AG reconstruction:

$$f_{12}(\mathrm{v}) = \rho_1 g(u; u_1, \sigma_1) g(v; a_0 + a_1 u, \sigma_2), \tag{3.4}$$

where the remaining parameters depend on the six moments contained inside the dashed frame in Figure 1. The indices of these moments live in $\mathcal{I}_{AG}$. It is interesting to note that in this limit $f_{12} = f_{21}$, and the same algorithm as described above for 2-D MG quadrature can be used to compute the six parameters $(\rho_1, u_1, \sigma_1, a_0, a_1, \sigma_2)$ in Eq. (3.4). In summary, the two limiting cases for high and low Stokes numbers are contained as special cases in the 2-D MG quadrature defined by Eq. (3.1).

3.3. *Regularization of σ*

The 1-D bi-Gaussian quadrature (Chalons *et al.* 2010) is an essential step for the 2-D MG quadrature. However, transition zones between mono-Gaussian and bi-Gaussian reconstructions were observed where a quadrature point is generated with high velocity but associated to a negligible density. As the CFL condition is based on the maximum velocity, this behavior will drastically reduce the time step. To avoid the generation of such high velocities, a regularization procedure is employed. The difference between the mean velocity of each Gaussian is given by $\Delta u = |u_2 - u_1| = q/(e - \sigma^2)$, where e and q are the centered moments of order 2 and 3†, while σ^2 is the variance of each Gaussian of the

† The centered moments e and q are defined from the considered univariate moments M_0, M_1, M_2 and M_3 by $e = (M_0 M_2 - M_1^2)/M_0^2$ and $q = (M_3 M_0^2 - 3M_0 M_1 M_2 + 2M_1^3)/M_0^3$.

reconstruction. Thus Δu is an increasing function of σ. If $\sigma = 0$, the velocity difference will be bounded (Chalons *et al.* 2012). Regularization consists of using a limiter on σ^2 to control the maximum velocity difference:

$$\sigma^2 = \begin{cases} \sigma^2 & \text{if } \Delta u < \Delta u_{lim} \\ e - \dfrac{|q|}{l} & \text{if } \Delta u \geq \Delta u_{lim}, \end{cases}$$

where

$$l = \Delta u_{lim} + (\Delta u_{max} - \Delta u_{lim}) \tanh\left(\frac{\Delta u - \Delta u_{lim}}{\Delta u_{max} - \Delta u_{lim}}\right). \tag{3.5}$$

The user-defined parameters Δu_{lim} and $\Delta u_{max} > \Delta u_{lim}$ represent the velocity difference after which a limitation holds and the maximum authorized velocity difference. In practice, these parameters must be close to the gas-phase velocity. The difference between Δu_{lim} and Δu_{max} allows a smooth transition between regularized and non-regularized zones. Note that in regularized zones only the fourth-order moment is not conserved by the reconstructed NDF.

4. Moment evolution

In the following, we describe how we use the MG quadrature introduced in the previous section to build realizable and efficient numerical methods to account for drag and advection. As we are using operator splitting, the drag force and advection in each direction are treated separately.

4.1. *Drag force*

For pure drag, a dimensional splitting is used even though the 2-D system (2.2) is closed. For the simple case of Stokes law, the drag term can be directly solved, but splitting will be important for more complex laws. The resulting equations corresponding to the x and y directions are

$$\partial_t M_{i,j} = \frac{i}{\tau_p}(M_{i-1,j}u_g - M_{i,j}), \qquad \partial_t M_{i,j} = \frac{j}{\tau_p}(M_{i,j-1}v_g - M_{i,j}). \tag{4.1}$$

Explicit analytical solutions of Eq. (4.1) are found assuming a constant gas velocity during the time step. To account for more complex physics (arbitrary drag laws, two-way coupling, etc.), we make use of the NDF reconstruction to derive a quadrature approximation of the source term. A Gauss-Hermite quadrature of f_{12} (conditioned on the first direction) is used for the drag equation corresponding to the x direction, and a Gauss-Hermite quadrature of f_{21} for the drag equation corresponding to the y direction.

4.2. *Kinetic-based flux-splitting scheme*

Here we present a numerical scheme applicable to all described methods (MG, CQMOM and AG) that makes use of the NDF reconstruction and an upwind resolution of the fluxes. As we use a dimensional splitting for advection, we derive the transport scheme for x direction only. The corresponding moment equations are

$$\begin{cases} \partial_t M_{i,j} + \partial_x M_{i+1,j} = 0, & \text{for } (i,j) \in \mathcal{I} \text{ and } (i+1,j) \in \mathcal{I} \\ \partial_t M_{i,j} + \partial_x \overline{M}_{i+1,j} = 0, & \text{for } (i,j) \in \mathcal{I} \text{ and } (i+1,j) \notin \mathcal{I} \end{cases}, \tag{4.2}$$

where overlined moments must be evaluated using the NDF reconstruction, and $\mathcal{I}$ is the set of moments needed for a particular reconstruction method. To describe the complexity

of the advective fluxes, a kinetic flux splitting scheme is proposed (Harten *et al.* 1983). First we consider a finite-volume formulation (where c is the cell index):

$$\mathbf{M}_c^{n+1} = \mathbf{M}_c^n - \frac{\Delta t}{\Delta x}\left(\mathbf{F}_{c+1/2} - \mathbf{F}_{c-1/2}\right). \tag{4.3}$$

The fluxes are decomposed into positive and negative parts:

$$\mathbf{F}_{c+1/2} = \mathbf{F}^+_{c+1/2} + \mathbf{F}^-_{c+1/2}. \tag{4.4}$$

Positive and negative components are obtained by integrating on $\mathbb{R}^+$ or $\mathbb{R}^-$ the NDF reconstruction f_{12}, here conditioned on the first direction x (symmetrically, for the transport scheme for y direction, f_{21} conditioned on the second direction y is used):

$$(F_{ij})^+_{c+1/2} = \int_v \int_0^\infty f_{12}(t, x_c, \mathrm{v}) u^{i+1} v^j \,\mathrm{d}u\,\mathrm{d}v, \tag{4.5}$$

$$(F_{ij})^-_{c+1/2} = \int_v \int_{-\infty}^0 f_{12}(t, x_{c+1}, \mathrm{v}) u^{i+1} v^j \,\mathrm{d}u\,\mathrm{d}v. \tag{4.6}$$

While this scheme is first order, higher-order schemes have been proposed for each method. For CQMOM, a quasi-second-order method was developed by Vikas *et al.* (2011) and a fully second-order method by Kah *et al.* (2011). For AG, a second-order method was developed by Vié *et al.* (2012*a*). Finally, for MG a second-order scheme is suggested by Chalons *et al.* (2010), based on what was done for CQMOM, applying an additional 16-node CQMOM quadrature on the moment set by reconstructing 48 moments using the MG quadrature. Another more robust alternative is to use the Gauss-Hermite quadrature for f_{12} together with the quasi-high-order scheme of Vikas *et al.* (2011). As this work is devoted to the first qualitative analysis of the proposed strategies (CQMOM, AG and MG), we will use the first-order scheme.

5. Results and discussion: frozen HIT

The proposed test case is a particle-laden gas phase represented by 2-D frozen homogeneous isotropic turbulence (HIT) generated with the ASPHODELE code of CORIA, which solves 2-D and 3-D low-Mach-number Navier-Stokes equations. The turbulence is generated following the Pope spectrum with parameters $p_0 = 4$, $c_L = 0.013$, $c_\eta = 0.105$ and $\beta = 5.2$ (Pope 2000). The particle phase is injected homogeneously in the domain at $t = 0$ with the same velocity as the gas phase. The droplet number density is constant and the Stokes number range based in the Kolmogorov time scale ($t_\eta = 0.3172$ s) is $\mathrm{St} = \tau_p/t_\eta \in [1, 20]$, which is large enough to observe trajectory crossings. Predicting this type of flows is important, as it is expected to exhibit the main effects of a turbulence gas field on a disperse liquid spray, i.e., the preferential concentration of particles in low vorticity zones that greatly influences auto-ignition, which is of primary importance for combustion applications. This effect is highly size dependent, so the test case is particularly interesting for quantifying the accuracy of the methods.

5.1. *Number density field*

The particle number density field $M_{0,0}$ is an important quantity in particle-laden flows that exhibit Stokes-number-dependent segregation. Thus, we are particularly interested to assess how well the Eulerian methods are able to capture the structure of $M_{0,0}$ for different Stokes numbers as compared to the Lagrangian method. In Figure 2, results are

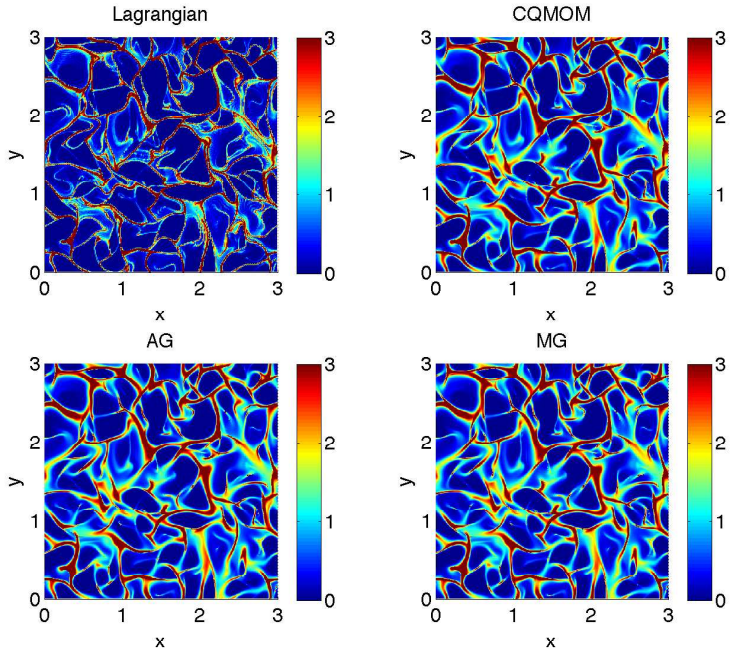

FIGURE 2. Number density for St = 1 from Lagrangian method with 65M particles (top right), CQMOM (top left), AG (bottom left) and MG (bottom right).

shown at $t = 4$, where segregation is effective for St = 1. For this Stokes number, PTC is minimal so that the second-order moments of the particle velocity fluctuations are small relative the mean particle velocity. As seen in Figure 2, the number density fields for all methods are quite similar and exhibit strong segregation. The observable small differences between the Lagrangian and Eulerian methods are mainly due to numerical diffusion associated with the first-order advection scheme. Indeed, Eulerian solutions on finer meshes show sharper boundaries between regions with and without particles.

In Figure 3, results are shown at $t = 4$ for St = 5. For this Stokes number, PTC is significant so that the second-order moments of the particle velocity fluctuations can be large relative to the mean particle velocity. As seen in Figure 3, the number density fields for the different methods all exhibit significant segregation, but now the fields for the Eulerian methods are clearly different. In general, the result found with CQMOM is closest to the Lagrangian field. Indeed, at some locations CQMOM predicts even higher concentrations than the Lagrangian method, which can be attributed to the weakly hyperbolic nature of this closure (i.e., leading to the formation of δ-shocks). At St = 5, most of the PTC is due to a single crossing event, which can be exactly resolved by CQMOM. In contrast, AG only conserves the second-order moments and PTC, with its potential intrinsic anisotropy, is modeled as a velocity dispersion generator at kinetic level and thus feeds with energy the related components of the covariance matrix. This results in a smoother number density field than is seen with quadrature-based moment methods. In comparison, in a similar way as CQMOM, MG is able to capture single crossing events but not multiple crossings. For this reason, the MG result at St = 5 is closer than AG to the Lagrangian reference field. Finally, we should also note that numerical diffusion

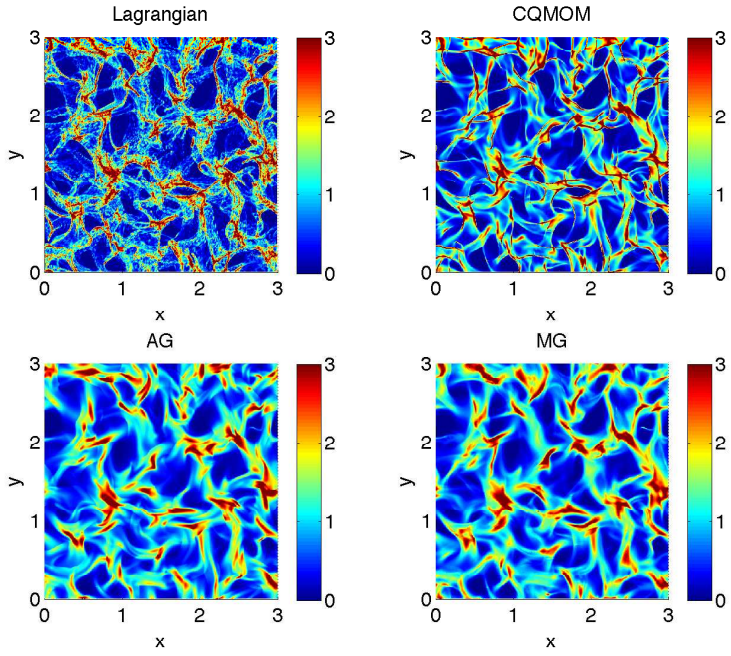

FIGURE 3. Number density for St = 5 from Lagrangian method with 65M particles (top right), CQMOM (top left), AG (bottom left) and MG (bottom right).

in the Eulerian methods will lead, in general, to smoothing of the number density fields. However, the δ-shocks in CQMOM will have an anti-diffusive effect since they tend to accumulate mass in non-physical narrow regions.

In Figure 4, results are shown at $t = 4$ for St = 20. As can be seen in the Lagrangian result, at larger Stokes numbers the particle velocities become more "random", leading to a less-segregated number density field and multiple PTC. The inability of CQMOM to resolve more than one PTC without forming δ-shocks is clearly observable in the relatively high segregation in the CQMOM number density field. Qualitatively, the MG result is closer to the Lagrangian field for this Stokes number. For even higher Stokes numbers, we expect that the MG and AG fields will become more similar since the particle velocity statistics will be nearly isotropic Gaussian (i.e., close to the initial conditions).

5.2. *Mean segregation*

While qualitative trends have been described above, we now focus on quantitative comparisons. The time evolution of the mean segregation is an important quantity and it is defined as $S = \langle M_{0,0}^2 \rangle / \langle M_{0,0} \rangle^2$ where $\langle \cdot \rangle$ denotes the spatial average. Then, $S = 1$ corresponds to a uniform field and $S = \infty$ to a highly segregated field composed of point masses. In Figure 5, the time evolution of the mean segregation with St = 1, 5 and 10 is shown for each method. As expected, the mean segregation is largest for St = 1 due to strong accumulation of particles in regions of low vorticity. In general, for St = 1 the Eulerian methods predict lower mean segregation because of numerical diffusion. In order to verify this assertion, a second-order AG result is included in Figure 5 and shows larger mean segregation than the first-order advection scheme (although still noticably smaller than the Lagrangian result).

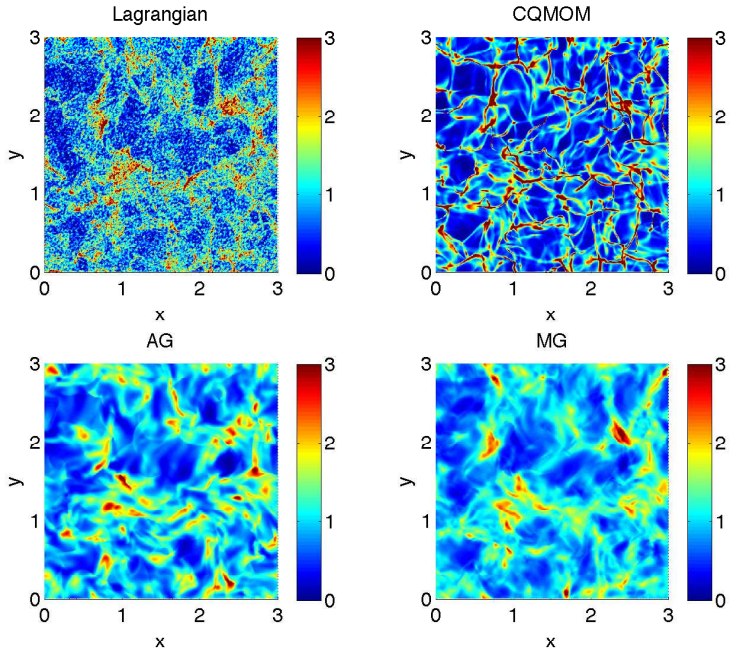

FIGURE 4. Number density for St = 20 from Lagrangian method with 65M particles (top right), CQMOM (top left), AG (bottom left) and MG (bottom right).

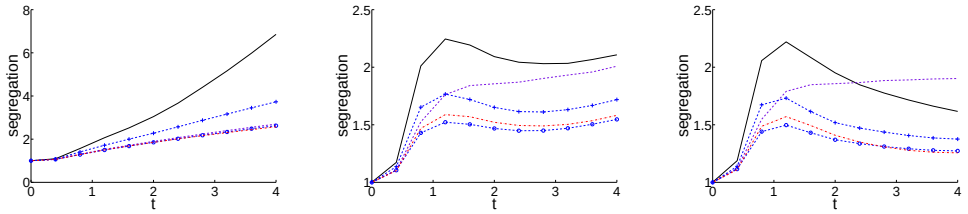

(a) St = 1 (b) St = 5 (c) St = 10

FIGURE 5. Time evolution of mean segregation from the Lagrangian method projected on a 256×256 mesh (black line), CQMOM (violet dashed line), AG (blue dashed line with o), AG with second-order discretization (blue dashed line with +) and MG (red dotted-dashed line).

For St = 5 and 10, the Lagrangian mean segregation reaches a maximum value before decreasing. This behavior is because of PTC. Except for CQMOM, the Eulerian methods generally follow the trend seen with the Lagrangian method, but at a lower level due to numerical diffusion. Indeed, with second-order advection a clear improvement is seen in the AG result. For CQMOM, the δ-shocks due to multiple PTC result in an overprediction of the mean segregation. In fact, with a higher-order advection scheme we would expect the CQMOM prediction for the mean segregation to be significantly larger than the Lagrangian result for large Stokes numbers. Overall, based on the mean segregation predictions, we can conclude that the MG method does the best job of reproducing the Lagrangian results and that further improvements could be made by implementing a second-order MG advection scheme.

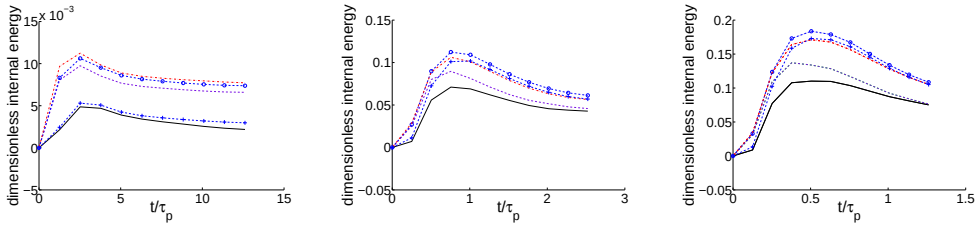

(a) St = 1 (b) St = 5 (c) St = 10

FIGURE 6. Time evolution of phase-average granular temperature from the Lagrangian method projected on a 256×256 mesh (black line), CQMOM (violet dashed line), AG (blue dashed line with o), AG with second-order discretization (blue dashed line with +) and MG (red dotted–dashed line).

5.3. *Granular temperature*

For fluid-particle systems, the granular temperature is defined in terms of the trace of the velocity covariance matrix: $\Theta_p = \left(M_{2,0} + M_{0,2} - (M_{1,0}^2/M_{0,0}) - (M_{0,1}^2/M_{0,0})\right)/(2M_{0,0})$ and is an indirect measure of the degree of local PTC in a particle-laden flow. In HIT, we can use the phase-average granular temperature $\widetilde{\Theta}_p = \langle M_{0,0}\Theta_p\rangle/\langle M_{0,0}\rangle$ as a global measure of PTC. In Figure 6, the time evolution of phase-average granular temperature, normalized using the RMS velocity of the gas phase, is shown with St = 1, 5 and 10 for each method. For all Stokes numbers, $\widetilde{\Theta}_p(t)$ first increases, passes through a Stokes-number-dependent maximum, and then decays. As expected, the maximum increases with St reflecting the increase in PTC. While all of the Eulerian methods capture the qualitative behavior of $\widetilde{\Theta}_p(t)$, the Lagrangian result is consistently smaller than the Eulerian results. As noted earlier, in moment methods numerical diffusion increases Θ_p and thus it is not surprising to find larger values of $\widetilde{\Theta}_p(t)$ with the Eulerian methods. At larger Stokes numbers, the better agreement of CQMOM with the Lagrangian results is due to the δ-shocks, which accumulate mass and destroy Θ_p in zones with multiple PTC.

5.4. *Granular energy*

Another important variable in fluid-particle flows is the phase-average granular energy, defined in a 2-D flow by $\widetilde{e}_p = \left(\langle M_{2,0}\rangle + \langle M_{0,2}\rangle\right)/(2\langle M_{0,0}\rangle)$. In HIT, the phase-average particle velocities are statistically zero, so that $\widetilde{e}_p$ is the sum of $\widetilde{\Theta}_p$ and the particle-phase turbulent kinetic energy k_p. In Figure 7, the time evolution of phase-average granular energy normalized using the RMS velocity of the gas phase is shown with St = 1, 5, 10 and 20 for each method. As expected, the behavior of $\widetilde{e}_p(t)$ depends strongly on the Stokes number. (In the limit St = 0, $\widetilde{e}_p(t) = \widetilde{e}_p(0) = k_p$ since $\widetilde{\Theta}_p = 0$.) For St = 1, $\widetilde{e}_p$ decreases slightly as particles segregate into zones with lower fluid-phase kinetic energy. Because $\widetilde{\Theta}_p$ remains very small for St = 1, we can conclude that the change in k_p follows that of $\widetilde{e}_p$. In contrast, for larger Stokes numbers the decrease in $\widetilde{e}_p(t)$ is much more pronounced. For St = 5, we can observe that $\widetilde{e}_p(t)$ nearly attains a steady-state value for the largest t, while for larger Stokes numbers this is not the case. Similar behavior is observed for $\widetilde{\Theta}_p(t)$ in Figure 6. However, for the granular energy the Eulerian methods are all in good agreement with the Lagrangian results. Because the granular energy is a conserved variable (which is not the case for $\widetilde{\Theta}_p$), this would indicate that the Eulerian methods correctly reproduce the drag terms $\langle M_{1,0}u_g\rangle$ and $\langle M_{0,1}v_g\rangle$ in the Reynolds-average moment transport equations.

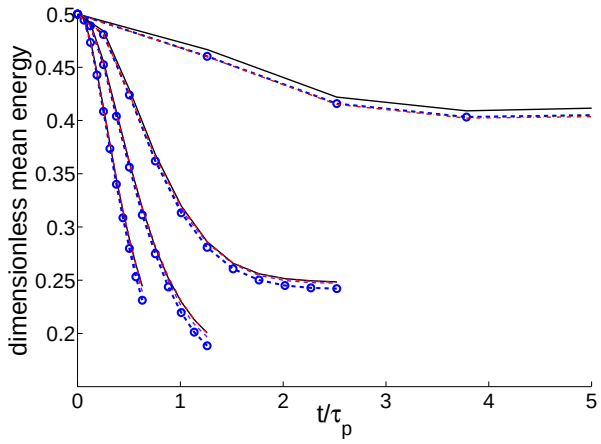

FIGURE 7. Time evolution of phase-average granular energy for St = 1 5, 10 and 20 (top to bottom) from Lagrangian method with 65M particles (black line), CQMOM (green line), AG (blue dots) and MG (red line).

6. Conclusions

The main goal of this work was to investigate three Eulerian moment methods as possible closure approaches for particle-laden flows over a wide range of Stokes numbers. Such methods, while investigated in the framework of DNS in the present work, will be an essential building block for LES modeling and simulations, which is going to rely strongly on present developments. Using Lagrangian simulations as a reference, the relative merits of the three methods were found to depend strongly on the Stokes number. For small St, the three methods performed quite similarly due to the absence of particle trajectory crossings. For medium and large Stokes numbers, the MG approach performs best due to its ability to capture both small-scale and large-scale PTC. In comparison with the Lagrangian results, the first-order advection schemes used with the Eulerian methods exhibit significant numerical diffusion, which is detrimental to their ability to predict the particle segregation. However, results found with a second-order advection scheme are encouraging and point to the need for further development of realizable high-order schemes. Nonetheless, the findings from this study allow us to conclude that Eulerian moment methods represent a promising alternative to Lagrangian methods for simulating particle-laden flows.

Acknowledgments

The authors wish to thank Parviz Moin and the Center for Turbulence Research at Stanford University for their hospitality and financial support during the 2012 CTR Summer Program. The support of the France-Stanford Center for Interdisciplinary Studies through a collaborative project grant (PIs: P. Moin / M. Massot), as well as the support from the RTRA DIGITEO (Project MUSE, PI M. Massot) and Ecole Centrale Paris for the postdoctoral fellowship of A. Vié are gratefully acknowledged. Part of the research leading to the results reported in this work was funded from the European Union Seventh Framework Programme (FP7/2007-2013) under grant agreement No. 246556.

REFERENCES

Chalons, C., Fox, R. O. & Massot, M. 2010 A multi-Gaussian quadrature method of moments for gas-particle flows in a LES framework. In *Proceedings of the Summer Program 2010, Center for Turbulence Research, Stanford University*, pp. 347–358.

Chalons, C., Kah, D. & Massot, M. 2012 Beyond pressureless gas dynamics: Quadrature-based velocity moment models. *Commun. Math. Sci.* **10**, 1241–1272.

Desjardins, O., Fox, R. O. & Villedieu, P. 2008 A quadrature-based moment method for dilute fluid-particle flows. *J. Comput. Phys.* **227** (4), 2514–2539.

Dombard, J. 2011 Direct Numerical Simulation of non-isothermal dilute sprays using the Mesoscopic Eulerian Formalism. PhD thesis, Université de Toulouse.

Février, P., Simonin, O. & Squires, K. D. 2005 Partitioning of particle velocities in gas-solid turbulent flow into a continuous field and a spatially uncorrelated random distribution: theoretical formalism and numerical study. *J. Fluid Mech.* **533**, 1–46.

Harten, A., Lax, P. D. & van Leer, B. 1983 On upstream differencing and Godunov-type schemes for hyperbolic conservation laws. *SIAM Rev.* **25** (1), 35–61.

Kah, D., Laurent, F., Fréret, L., de Chaisemartin, S., Fox, R., Reveillon, J. & Massot, M. 2010 Eulerian quadrature-based moment models for dilute polydisperse evaporating sprays. *Flow, Turb. and Combustion* **85**, 649–676.

Kah, D., Vié, A., Chalons, C. & Massot, M. 2011 Second order scheme for quadrature-based velocity high order moment methods for disperse two-phase flows. *Annual Research Briefs, Center for Turbulence Research, Stanford University* pp. 321–334.

Kaufmann, A., Moreau, M., Simonin, O. & Helie, J. 2008 Comparison between Lagrangian and mesoscopic Eulerian modelling approaches for inertial particles suspended in decaying isotropic turbulence. *J. Comput. Phys.* **227** (13), 6448–6472.

Masi, E., Simonin, O. & Bédat, B. 2011 The mesoscopic Eulerian approach for evaporating droplets interacting with turbulent flows. *Flow, Turb. and Combustion* **86**, 563–583.

Pope, S. B. 2000 *Turbulent Flows*. Cambridge: Cambridge University Press.

Sierra, P. 2012 Modeling the dispersion and evaporation of sprays in aeronautical combustion chambers. PhD thesis, INP Toulouse.

Vié, A., Chalons, C., Fox, R. O., Laurent, F. & Massot, M. 2011 A multi-Gaussian quadrature method of moments for simulating high-Stokes-number turbulent two-phase flows. *Annual Research Briefs, Center for Turbulence Research, Stanford University* pp. 309–320.

Vié, A., Doisneau, F., Laurent, F. & Massot, M. 2012*a* On the Anisotropic Gaussian closure for the prediction of inertial-particle laden flows. *Comm. in Comp. Phys.* pp. 1–18, submitted.

Vié, A., Masi, E., Simonin, O. & Massot, M. 2012*b* On the direct numerical simulation of moderate-Stokes-number turbulent particulate flows using Algebraic-Closure-Based and Kinetic-Based Moment Methods. In *Proceedings of the Summer Program 2012, Center for Turbulence Research, Stanford University*, pp. 355–364.

Vikas, V., Wang, Z. J., Passalacqua, A. & Fox, R. O. 2011 Realizable high-order finite-volume schemes for quadrature-based moment methods. *J. Comput. Phys.* **230** (13), 5328–5352.

Yuan, C. & Fox, R. O. 2011 Conditional quadrature method of moments for kinetic equations. *J. Comput. Phys.* **230** (22), 8216–8246.